Journal of
Ship&Ocean
Technology
©June 2000

SOTECH Vol. 4, No. 2, pp. 13 ~ 23, 2000

Modified Split Panel Method Applied to the Analysis of Cavitating Propellers

S.-W. Pyo[1] and J.-C. Suh[1]

[1] Department of Naval Architecture and Ocean Engineering, Seoul National University, San 56-1, Shinrim-dong, Kwanak-ku, Seoul, 151-742, KOREA; E-mail: pyo@cavity.snu.ac.kr

Abstract

A low-order potential based boundary element method is applied to the prediction of the flow around the cavitating propeller in steady or in unsteady inflow. For given cavitation number, the cavity shape is determined in an iterative manner until the kinematic and the dynamic boundary conditions are both satisfied on the approximate cavity boundary. In order to improve the solution behavior near the tip region, a hyperboloidal panel geometry and a modified split panel method are applied. The method is then extended to include the analysis of time-varying cavitating flows around the propeller blades via a time-step algorithm in time domain. In the method, the steady state oscillatory solution is obtained by incremental stepping in the time domain. Finally, the present method is validated through comparison with other numerical results and experimental data.

Keywords: propeller, cavitation, unsteady, boundary element method

1 Introduction

Propeller cavitation is becoming more and more common in recent ocean vehicle applications. In the past, the propeller design philosophy has been to avoid cavitation for the widest possible range of operating conditions. However, recent demands for higher vehicle speeds and higher propeller loads have made this design philosophy practically impossible to achieve. The alternative is to allow for controlled amounts of sheet cavitation, which is less harmful than other types of cavitation (bubble or cloud cavitation) and to design propellers with small blade area. Computational methods for the analysis of the propeller sheet cavitation in nonuniform or in uniform inflow have been developed. Boundary Element methods(BEM) have been found to be a computationally efficient, robust tool for the analysis of cavitating propellers (Fine 1992, Kim and Lee 1996) as well as non-cavitating propellers (Lee 1987). These methods employ either a potential or a velocity based formulation. The investigation of different panel methods showed that the iterative process in a potential based BEM for finding the cavity shape converged much more quickly than in a velocity based BEM (Kinnas and Fine 1993). A perturbation potential based BEM for the analysis of the partially cavitating hydrofoils in two or three dimensions was developed (Kinnas and Fine 1993). For a given cavitation number, the cavity shape was determined by satisfying both the kinematic and the dynamic boundary conditions on the cavity boundary. It was found that the cavity solution even from the first iteration was very close to the fully nonlinear converged solution (Kinnas and

Fine 1993). The method was then extended to include the effect of the supercavitation and to the analysis of time-varying cavitating flows around the propeller blades (Fine 1992). To save computating time, a split panel method was also applied. The BEM has been applied successfully for the analysis of the partially or super-cavitating propellers. However, most methods did not apply a numerical Kutta condition because of its complexity and the method often has difficulty with converging near the blade tip region because of high skewness of the panels and the error from the split panel method (Fine 1992). In the present work, a method is presented to take into account all of the above. In addition. the Kutta condition suggested by Suh et al (1992) is implemented numerically in the method. To improve the convergence near the blade tip region, hyperboloidal panels are used for the panel representation of the blade surface and a modified split panel method is developed.

2 Mathematical Formulation

Consider a partially- or super-cavitating propeller, shown in Figure 1, subject to a spatially nonuniform inflow $U_\infty(y,z,t)$. The perturbation potential $\phi_p(t)$ at any time t and any point p on the wetted surface $S_{WS}(t)$ or the cavity surface $S_C(t)$ may be expressed by using Green's third identity (Kinnas and Fine 1993):

$$\begin{aligned} 2\pi\phi_p(t) &= \int_{S_{WS}(t)\cup S_C(t)} \left[\phi_q(t)\frac{\partial}{\partial n_q(t)}\left(\frac{1}{R(p;q)}\right) - \frac{\partial\phi_q}{\partial n_q}(t)\frac{1}{R(p;q)}\right] dS \\ &+ \int_{S_W(t)} \Delta\phi_w(t)\frac{\partial}{\partial n_q(t)}\left(\frac{1}{R(p;q)}\right) dS \end{aligned} \tag{1}$$

where q corresponds to the variable point in the integrations and the unit normal vector $n_q(t)$ to the wetted surface of the propeller blade, the cavity surface and the trailing wake surface $S_W(t)$ points into the fluid. $R(p;q)$ is the distance from the q to the point p and $\Delta\phi_w(t)$ is the potential jump across the trailing wake surface.

To determine the unique potential flow solution, the boundary conditions have to be applied on the flow boundaries. However, since the geometry of the cavity surface is unknown, as initial flow boundaries, the cavity surface $S_{CB}(t)$ on the blade is approximated by the blade surface, and the cavity surface in the wake $S_{CW}(t)$ is approximated by the wake surface. Since the normal velocity is discontinuous across $S_{CW}(t)$, the velocity jump can be defined as a source distribution of density $q_w(t)$:

$$q_w(t) = \frac{\partial\phi_q}{\partial n_q}^{+}(t) - \frac{\partial\phi_q}{\partial n_q}^{-}(t) \tag{2}$$

Depending on the location of the field point p, which may either be on $S_{WS}(t) \cup S_{CB}(t)$ or on $S_{CW}(t)$, the equation (1) can be rewritten and each case may be considered separately.

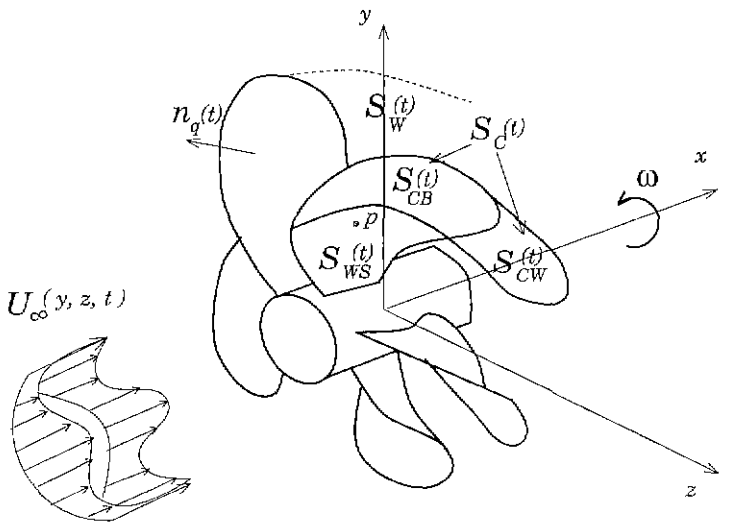

Figure 1: Definition of flow boundaries.

- **Field point on $S_{WS}(t) \cup S_{CB}(t)$:**
  Substituting (2) into (1), we obtain

$$
\begin{aligned}
2\pi\phi_p(t) &= \int_{S_{WS}(t)\cup S_{CB}(t)} \left[\phi_q(t)\frac{\partial}{\partial n_q(t)}\left(\frac{1}{R(p;q)}\right) - \frac{\partial\phi_q}{\partial n_q}(t)\frac{1}{R(p;q)}\right] dS \\
&\quad - \int_{S_{CW(t)}} q_w(t)\frac{1}{R(p;q)} dS \\
&\quad + \int_{S_{CW(t)}\cup S_W(t)} \Delta\phi_w(t)\frac{\partial}{\partial n_q(t)}\left(\frac{1}{R(p;q)}\right) dS
\end{aligned} \tag{3}
$$

  where superscripts $+, -$ correspond to the upper and lower side of the wake surface, respectively.

- **Field point on $S_{CW}(t)$:**
  Consider the field point is on the upper and the lower side of $S_{CW}(t)$. By adding the equations and noting that the potential jump across the wake sheet $\Delta\phi_w(t) = \phi_p^+(t) - \phi_p^-(t)$, we obtain from (1)

$$
\begin{aligned}
4\pi\phi_p^+(t) &= 2\pi\Delta\phi_w(t) + \int_{S_{WS}(t)\cup S_{CB}(t)} \left[\phi_q(t)\frac{\partial}{\partial n_q(t)}\left(\frac{1}{R(p;q)}\right) - \right. \\
&\quad \left. \frac{\partial\phi_q}{\partial n_q}(t)\frac{1}{R(p;q)}\right] dS - \int_{S_{CW(t)}} q_w(t)\frac{1}{R(p;q)} dS \\
&\quad + \int_{S_{CW(t)}\cup S_W(t)} \Delta\phi_w(t)\frac{\partial}{\partial n_q(t)}\left(\frac{1}{R(p;q)}\right) dS
\end{aligned} \tag{4}
$$

Equations (3) and (4) express the potential $\phi_p(t)$ on the blade surface or the potential $\phi_p^+(t)$ on the wake surface as the superposition of the potentials induced by a continuous source distribution on the wetted and the cavity surface, and a continuous dipole distribution on the wetted and cavity surface as well as on the wake surface. These source and dipole strengths can be uniquely determined by solving (3), (4) along with the following boundary conditions:

- **Kinematic boundary condition** on the non-cavitating surface: This condition defines the source strength on the non-cavitating surface as follows:

$$\frac{\partial \phi_q}{\partial n_q}(t) = -\vec{U}_\infty(y,z,t)\cdot\hat{n}_q(t) \tag{5}$$

- **Dynamic boundary condition** on the cavity surface: The pressure on the cavity surface should be constant and equal to a given cavitation pressure p_c. By applying Bernoulli's equation in a propeller fixed coordinate system, the potential $\phi(s,v,t)$ on the cavity surface can be obtained (Fine 1992). Since cavitation may occur on the blade surface or on the wake surface, each boundary condition should be considered separately.

  (a) On the cavitating part of the blade,

$$\phi(s,v,t) = \phi(0,v,t) + \int_0^s \left[-U_s + \left(\frac{\partial\phi}{\partial v} + U_v\right)\cos\theta + \sin\theta \times \right.$$
$$\left. \sqrt{n^2D^2\sigma + |U_\infty(y,z,t)|^2 + \omega^2 r^2 - 2gY - 2\frac{\partial\phi}{\partial t} - \left(\frac{\partial\phi}{\partial v} + U_v\right)^2} \right] ds \tag{6}$$

  where s, v are the coordinates along the chordwise and the radial direction on the cavity surface, respectively and θ is the angle between s and v coordinates. U_s, U_v are the s, v components of the inflow relative to the propeller($U_\infty(y,z,t) + \omega \times r$), g is the gravitational constant, n is the number of propeller revolutions per second, D is the propeller diameter, σ is the cavitation number $((p_0 - p_c)/(1/2\rho n^2 D^2)$ and Y is the vertical distance from the axis of rotation and is defined as negative in the direction of the gravity.

  (b) On the cavitating part of the wake,

$$\phi^+(s,v,t) = \phi(0,v,t) + \int_{s_{TE}}^s [-U_s + \sqrt{n^2D^2\sigma + |U_\infty(y,z,t)|^2 + \omega^2 r^2 - 2gY - 2\frac{\partial\phi}{\partial t}}\,] ds \tag{7}$$

- **Kinematic boundary condition** on the cavity surface: The normal velocity on the cavity surface should be zero. From this condition, the partial differential equation for the cavity hight h is obtained (Fine 1992).

(a) On the cavitating part of the blade,

$$\frac{\partial h}{\partial s}\left[\left(U_s+\frac{\partial \phi}{\partial s}\right)-\cos\theta\left(U_v+\frac{\partial \phi}{\partial v}\right)\right]+$$
$$\frac{\partial h}{\partial v}\left[\left(U_v+\frac{\partial \phi}{\partial v}\right)-\cos\theta\left(U_s+\frac{\partial \phi}{\partial s}\right)\right]=\sin^2\theta\left[\left(U_n+\frac{\partial \phi}{\partial n}\right)-\frac{\partial h}{\partial t}\right] \quad (8)$$

(b) On the cavitating part of the wake,

$$\frac{\partial h}{\partial s}\sqrt{n^2D^2\sigma+\left|U_\infty(y,z,t)\right|^2+\omega^2r^2-2gY-2\frac{\partial \phi}{\partial l}}=q_w(t)-\frac{\partial h}{\partial t} \quad (9)$$

- **Kutta condition**: A numerical Kutta condition is applied to specify the circulation around the propeller blade at each time step, which is equal to the potential jump in the wake surface. The details of the condition is given in Suh et al(1992).

3 Numerical implementation

In solving (3), (4), the propeller blade is discretized into hyperboloidal panels. The time domain is also discretized into equal time interval Δt. For the trailing wake geometry, a nonlinear wake model is applied (Greeley and Kerwin 1982) and the wake surface is discretized into panels at constant angular interval $\Delta\theta(=\omega\Delta t)$. The algorithm for solving the unsteady cavitating propeller problem is as follows.

(a) First of all, the unsteady non-cavitating problem has to be solved. The stepwise solution algorithm is applied (Kim et al 1997) and the perturbation potentials are obtained at every time step. These values will be used for the calculation of the right hand side of (3), (4).

(b) For a given cavitation number and on the assumed cavity surface, we need to solve the following equation to find the correct cavity planform.

$$\delta_m(l_1,l_2,\cdots,l_M) = 0, \qquad m=1,\cdots,M \quad (10)$$

where δ_m is the cavity height at the cavity trailing edge of the m-th spanwise strip which is nondimensionalized by a local chord length c_m, and l_m is the cavity length at the same strip. An iterative procedure is required to solve (10) due to its nonlinear character. Equation (10) may be solved by applying an M-dimensional Newton-Raphson method. However since this method requires excessive computating time, a locally scalar Newton-Raphson method, which ignores the off diagonal terms of the Jacobian, is used in this work. Applying a locally scalar method at each strip, the cavity length of the i-th strip at $(k+1)$-th iteration may be expressed:

$$l_i^{k+1} = l_i^k-\frac{\partial l_i}{\partial \delta_i}\delta_i^k \qquad m=1,\cdots,M \quad (11)$$

For each iteration, the cavity height can be determined by the kinematic boundary condition, given in (8), (9). At each time step, the cavity planform is considered to be converged when

the maximum of the absolute values of δ is less than 0.001. The details of the method is described in Fine (1992).

From the iterative procedure, the boundary conditions are satisfied on the assumed cavity surface. In order to find the exact cavity surface, this iterative procedure has to be be repeated. However, it is known that the solution on the assumed cavity surface is very close to the fully nonlinear solution on the exact cavity surface (Kinnas and Fine 1993). In the present work, only one iterative procedure will be applied to find the solution.

(c) Step (b) continues for the next time step and until a steady state oscillatory solution is obtained. It usually takes three revolutions.

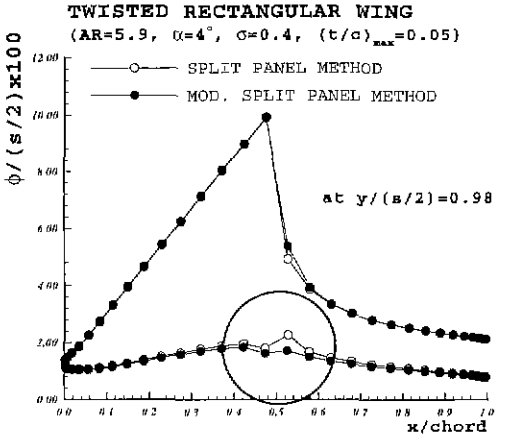

Figure 2: Comparison of the potentials computed by the split panel method with that by the modified split panel method. Computations are for an NACA65A twisted foil with $t/c = 0.05, AR = 5.9, \sigma = 0.4, \alpha = 4^o$.

4 Modified split panel method

Usually, the trailing edge of the cavity does not coincide with a panel boundary in the chordwise direction. Since only an integral number of panel can be used in the method, this may cause a problem. To avoid this problem, we need to re-panel the blade surface or use the split panel method, in which the panel at the trailing edge of the cavity is split into a cavitating(l_L) and a non-cavitating part(l_R). When the blade surface is re-paneled so that the cavity trailing edge coincides with a panel boundary , it is necessary to recompute all the influence coefficients. On the other hand. the split panel method can be applied without the added burden of recomputing influence coefficients (Fine 1992). In this method, the source strength $(\left(\frac{\partial\phi}{\partial n}\right)_R)$ on the non-cavitating part of a split panel and the dipole strength (ϕ_L) on the cavitating part of a split panel are known from (5), (6) while the source strength $(\left(\frac{\partial\phi}{\partial n}\right)_L, q_{wL})$ on the cavitating part of a split panel and the dipole strength (ϕ_R) on the non-cavitating part of a split panel are unknown and extrapolated from the knowns on adjacent panels. The details of the method is expressed in Fine(1992). Although

this method was applied with some success, it was found that it is often difficult for the solution to converge near the tip of the blade. To resolve this problem, we begin with the investigation of the perturbation potentials near the tip of the blade, which is shown in Figure 2. From this figure, it was concluded that as the thickness of the blade decreases, the influence of the split panel on the opposite panel on the pressure side of the blade becomes larger. Therefore, the effect of the spilt panel should be included in the potential calculation not by the extrapolation but by the introduction of an additional unknown. To implement this, we developed a *modified split panel method*, in which only the source strength $(\left(\frac{\partial \phi}{\partial n}\right)_L, q_{wL})$ on the cavitating part of a split panel is extrapolated from the known values on adjacent panels. The dipole strength (ϕ_R) on the non-cavitating part of a split panel is treated as an additional unknown. The resulting potentials from the modified split panel method are shown in Figure 2. Comparing the result with that from the original split panel method, it indicates that the ϕ_R extrapolation is not necessary.

5 Numerical results

The present method is applied to number of lifting surface configurations. Two groups of applications are presented. The first group is for a series of wings in uniform inflow and the second group is for a series of propellers in nonuniform as well as in uniform inflow. The results are compared to those from other numerical methods and to published experimental measurements.

5.1 Partially- or super-cavitating wing

In all calculations, the panels on the wing are distributed using cosine spacing in the chordwise and the spanwise direction. In the wake, panels are distributed using cosine spacing in the spanwise and the streamwise direction to emphasize the details near the blade trailing edge and the tip. The wing is discretized into 60 chordwise and 20 spanwise panels. The trailing wake sheet is discretized into 20 spanwise and 120 streamwise panels. The initial guess of the cavity geometry was a uniform cavity length$(l(y) = 0.8)$ at all spanwise positions.

- **Partially cavitating wing**
  Comparisons with the experimental measurement (Kinnas and Fine 1993) are made in this example. The experiment was performed at the MIT cavitation tunnel and the angle of attack was 6.5^o and the flow speed was $6.83m/s$. The cavitation numbers σ were 1.084 and 1.148. The cavity detachment point was taken at 2.4% of the local chord length. The comparison between the computational results and the experimental measurements are shown in Figure 4. For two cavitation numbers, predicted cavity planforms agree well with experiments.

- **Super-cavitating wing**
  The method is applied to a rectangular wing of aspect ratio $AR = 5.9$ at $\alpha = 3^o$. The wing has an NACA65A section with $\left(\frac{t}{c}\right)_{max} = 0.05$ at the midspan, tapering elliptically to zero at the tips. Figure 3 shows the converged cavity planform. The tolerance δ of the cavity height to the local chord length was set 0.001. Note that the cavity planform agrees fairly well with those from Fine(1992).

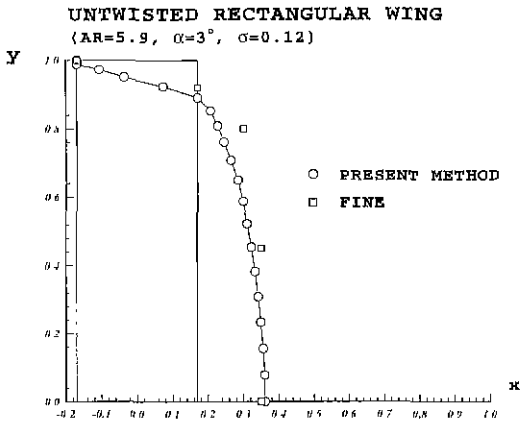

Figure 3: Cavity planform for a NACA65A rectangular foil with $t/c = 0.05, AR = 5.9, \sigma = 0.4, \alpha = 3^o$.

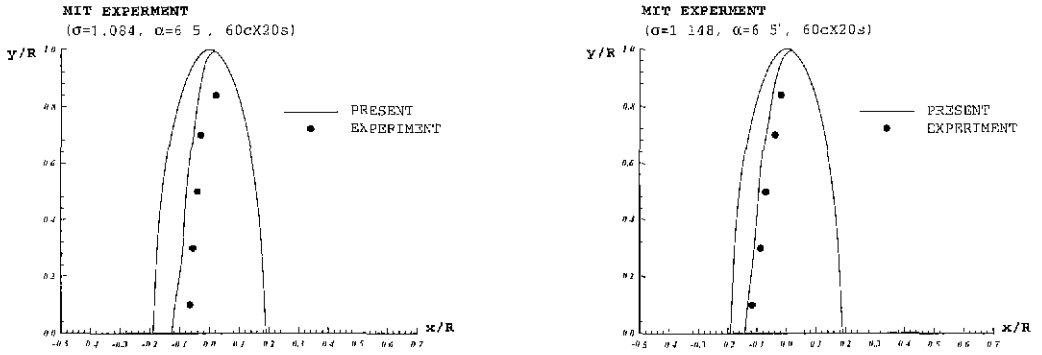

Figure 4: Cavity planform comparison for $\sigma = 1.084, 1.148$.

5.2 Partially- or super-cavitating propeller in a uniform inflow

The present method is applied to propellers in the same manner as in the case of the wings. The difference between this computation and that for the wing is that each trailing vortex is now assumed to travel in a helical trajectory rather than a straight line downstream. Also for the far field calculation, a sink disk is used instead of vortex lines, which were used in the wing problem. The far field calculation starts at $x = 1.5R$, which is usually used in the propeller application (Greeley and Kerwin 1982). The propeller blade is discretized into 60 chordwise and 20 radial panels. The initial guess of the cavity geometry was a uniform cavity length($l(y) = 0.8$) at all radial positions.

- **Partially cavitating propeller**
  The first case is for a propeller DTMB 4381. The propeller geometry is given in Fine(1992). The propeller is assumed to have one blade and operating in uniform inflow with an advance ratio $J_S = 0.8$ and a cavitation number $\sigma = 2.7$. The cavity detachment point is set at

2.4% of the local chord length after the leading edge. Figure 5 shows the converged cavity planform along with other numerical result (Fine 1992). Both cavity planforms show good agreement.

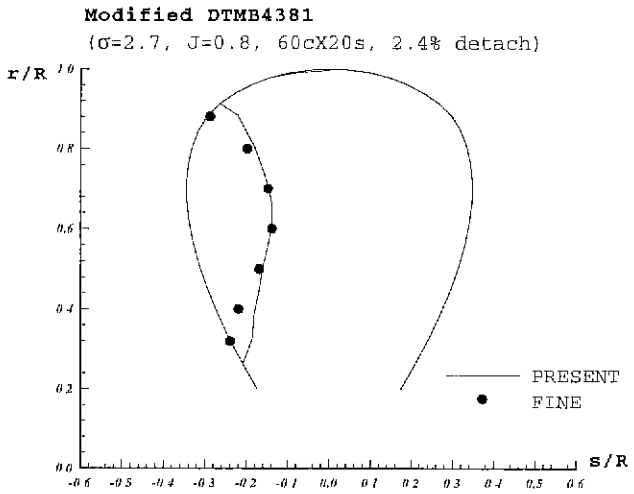

Figure 5: Expanded cavity planform for the modified DTMB 4381 propeller with one blade; $J_S = 0.8, \sigma = 2.7$.

- **Super-cavitating propeller**
  In order to examine the steady supercavity solution, the AO-177 propeller is calculated, whose geometry is given in Fine(1992). The propeller is assumed to have one blade and operating in uniform inflow with an advance ratio $J_S = 0.6$ and a cavitation number $\sigma = 2.5$. In this case, the cavity is assumed to detach at the leading edge of the blade. The converged cavity planform obtained by the present method is compared with the other numerical result (Fine 1992) are shown in Figure 6. Both cavity planforms show good agreement except the tip region. In Fine's method, the solution for the cavity planform is converged only for $\frac{r}{R} \geq 0.98$ while in the present method, the solution converged everywhere.

5.3 Cavitating propeller in nonuniform inflow

Finally, in order to validate the present method in nonuniform inflow, the method is applied for a modified DTMB 4381 propeller with one blade. The inflow has a 15% dent in axial direction and is symmetric about $\theta = 0^o$. The coefficients of the sine and cosine series are given in Fine(1992). The other components of the inflow are zero. Figures 7, 8 show the converged cavity planforms and volumes at different angular positions of the propeller. In Figure 8, the cavity volumes from the present method are compared to that from other numerical result (Lee 1979) at the second revolution. Those results show good agreement.

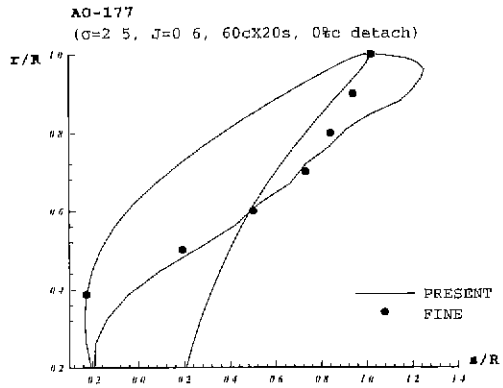

Figure 6: Expanded cavity planform for the one bladed AO-177 propeller; $J_S = 0.6, \sigma = 2.5$.

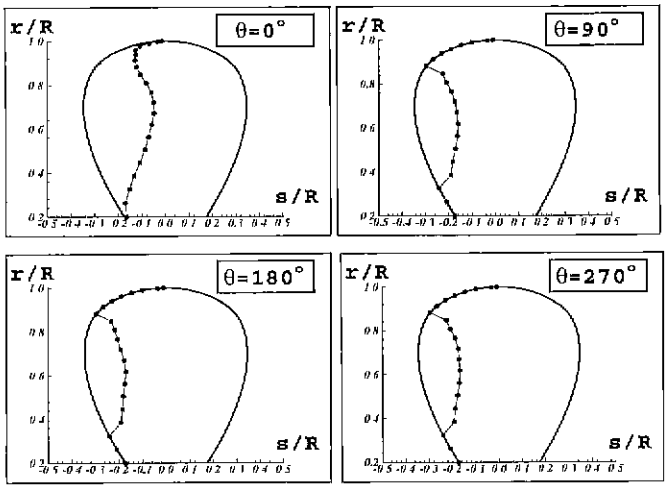

Figure 7: Cavity planform at different angular positions on the DTMB 4381 at $J_S = 0.8, \sigma = 2.7$.

6 Conclusions

In the present work, a computationally efficient and robust boundary element method for cavitating propellers in steady and unsteady inflow is developed. The unsteady problem is solved in the time domain and a stepwise solution algorithm with an efficient numerical Kutta condition is implemented at each time step. Since the first iteration solution has been shown to be very close to the converged nonlinear solution, only the first iteration is done to obtain a nonlinear solution. Both the fully wetted and the cavity solutions are found on a fixed panel discretization, so that the influence coefficients need to be calculated once. By employing hyperboloidal panels and the modified split panel method, the results from the present method show better convergence near the tip region than other numerical method.

The method is applied to number of cavitating wings and propellers in uniform and nonuniform

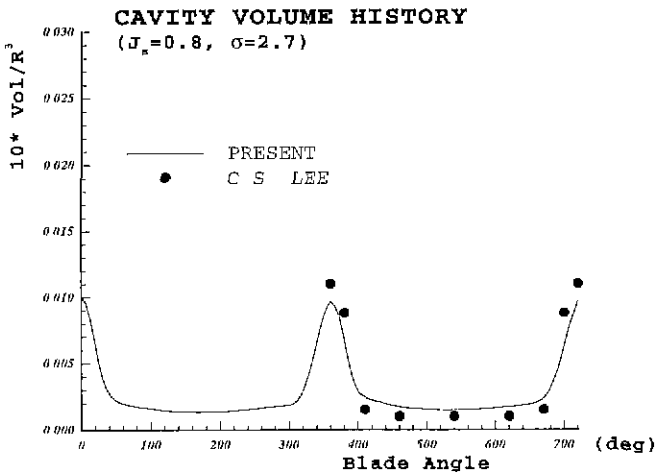

Figure 8: Cavity volume histories on the DTMB 4381 at $J_S = 0.8, \sigma = 2.7$.

inflow. The results are shown to agree with those from other numerical methods and published experimental measurements.

References

FINE, N.E. 1992 Nonlinear analysis of cavitating propellers in nonuniform inflow. MIT, Dept. of Ocean Engineering Report, **92-5**

GREELEY, D.S. AND KERWIN, J.E. 1982 Numerical methods for propeller design and analysis in steady flow. Trans, Society of Naval Architects and Marine Engineers, **90**

KIM, K., PYO, S. AND SUH, J.C. 1997 The analysis of marine propellers in unsteady flow. Proc, Annual Meeting, Society of Naval Architects of Korea, Seoul, November 1997, pp. 262-265

KIM, Y.-G. AND LEE, C.-S. 1996 Prediction of unsteady performance of marine propellers with cavitation using surface-panel method. Proc, 21st Symp on Naval Hydrodynamics, **IV**, pp. 16-31

KINNAS, S.A. AND FINE, N.E. 1993 A numerical nonlinear analysis of the flow around two- and three-dimensional partially cavitating hydrofoils. J. of Fluid Mechanics, **254**, pp. 151-181

LEE, C.-S. 1979 Prediction of steady and unsteady performance of marine propellers with or without cavitation by numerical lifting surface theory. PhD Thesis, MIT, Department of Ocean Engineering

LEE, J.T. 1987 A potential based panel method for the analysis of marine propellers in steady flow. PhD Thesis, MIT, Department of Ocean Engineering

SUH, J.C., LEE, J.T. AND SUH, S.B. 1992 A bilinear source and doublet distribution over a planar panel and its applications to surface panel methods. Proc, 19th Symp on Naval Hydrodynamics